Shahid Chamran University of Ahvaz

Iranian Association of Electrical and Electronics Engineers

Journal of Applied Research in Electrical Engineering

E-ISSN: 2783-2864
P-ISSN: 2717-414X
Homepage: https://jaree.scu.ac.ir/

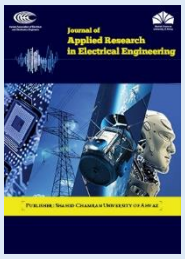

Research Article

Re-examination of the Doubly Fed Induction Machine (DFIM) Model Taking Into Account the Rotor Reactive Power

Mohammad Naser Hashemnia *

Department of Electrical Engineering, Mashhad Branch, Islamic Azad University, Mashhad, Iran

** Corresponding Author: hashemnia@mshdiau.ac.ir*

Abstract: Modeling electric machines is crucial for analyzing their behavior and designing controllers. It is of the utmost importance to make use of a consistent equivalent circuit of the Doubly Fed Induction Machine (DFIM) that is applicable to a variety of operating modes. This is because it helps in the calculation of the machine's steady-state performance, converter ratings, and controller set-points. Traditional models of doubly fed induction machines employ the steady-state equivalent circuit of a wound-rotor induction machine with all rotor parameters referred to the stator through a frequency conversion. The present study investigates the validity of the traditional steady-state circuit model by taking into account the sequence change in rotor voltages and currents at super-synchronous speeds. The validity of phasor diagrams constructed using the traditional circuit is assessed, with a particular focus on super-synchronous operation in both motoring and generating modes. It has been demonstrated that the existing model is applicable to all rotor speeds (whether sub-synchronous or super-synchronous). However, caution should be exercised when utilizing expressions of rotor reactive power that involve dynamic *dq* and steady-state phasor models. Therefore, modified expressions are developed for rotor reactive power that are applicable regardless of the operating speed. The accuracy of the proposed method for different operating modes is confirmed by comprehensive simulation results developed with Matlab® Simulink. An investigation is also conducted into the sensitivity of rotor reactive power direction to parameter changes, and it is shown that machine parameter changes have a negligible effect on rotor reactive power direction.

Keywords: Doubly Fed Induction Machine (DFIM), dynamic model, phasor diagram, reactive power, super-synchronous speed.

Article history
Received 16 August 2023; Revised 06 December 2023; Accepted 24 December 2023; Published online 29 January 2024.

How to cite this article
M. N. Hashemnia, "Re-examination of the Doubly Fed Induction Machine (DFIM) model taking into account the rotor reactive power," *J. Appl. Res. Electr. Eng.*, vol. 2, no. 2, pp. 182-193, 2023.
DOI: 10.22055/jaree.2023.44572.1078

Check for updates

1. INTRODUCTION

1.1. Research Motivation

Wind energy conversion systems utilizing a Doubly Fed Induction Machine (DFIM) are by far the most prevalent topology worldwide [1]. This is due to the numerous benefits of DFIMs, such as decoupled control of active and reactive powers, the use of a partial scale converter resulting in reduced costs and losses, and so forth [2]. Significant research has been conducted on this topology for grid-connected and stand-alone applications, and the mathematical relationships of the machine are well-established [3–8]. Besides the generation mode of DFIM operation, a number of applications have emerged in which the aforementioned benefits make DFIM an excellent candidate for the motoring mode of operation, including traction systems, marine propulsion and hybrid electric aircrafts [9-12]. A study of the machine's steady-state operation is essential for determining its steady-state characteristics and establishing the initial conditions for simulating its dynamic performance. In addition, sizing the converters necessitates a study of the active and reactive power ratings, which can be obtained most easily with the aid of equivalent circuit model equations [13]. Calculating the reference values of variables used as set-points in control loops requires valid and accurate model equations. Finally, load flow analysis of power systems with high penetration of wind turbines equipped with Doubly Fed Induction Generators (DFIGs) necessitates revisiting the traditional algorithms by taking the stator and rotor side

active/reactive powers into account [14-18]. Consequently, a consistent equivalent circuit that is applicable to various operating modes must be developed. Doubly fed induction generators (DFIGs) have been used predominantly in sub-synchronous mode, with super-synchronous operation restricted to wind gust conditions [19]. As demonstrated in [19], however, operation above synchronous speed results in higher efficiency, greater total output power and a simpler, less expensive power converter. Consequently, it is of the utmost significance to investigate DFIM in super-synchronous mode of operation. The super-synchronous study of DFIMs presents a challenge due to the appearance of negative values in the frequency of rotor circuit variables. The analysis of this issue can be traced back to 1983 [20], when a proposition was made to avoid referring the rotor circuit to the stator side and instead directly manipulate the rotor quantities at the rotor side. Nevertheless, the widely accepted representation of DFIMs is the stator-referred equivalent circuit. This choice is motivated by the desire to work with a circuit that encompasses a single frequency, namely the stator frequency, as opposed to a circuit that involves two different frequencies, namely the stator and rotor frequencies.

1.2. Literature Review

It has been claimed in [21, 22] that the traditional steady-state equivalent circuit exhibits deficiencies when employed in the super-synchronous mode of operation. A revised version of the model (referred to as the "accurate equivalent circuit" in references [21, 22]) is subsequently suggested for utilization in scenarios involving super-synchronous speeds, as an alternative to the widely accepted DFIM model. In effect, these references emphasize that the equivalent circuit structure depends on the rotor slip. This claim is supported by the change in the phase sequence of rotor variables at super-synchronous speeds, which influences the reactive power exchanged on the rotor side. The same authors put forward an iterative approach for integrating a DFIG into load flow analysis by utilizing its equivalent circuit in [23]. In [24], the same equivalent circuit was used to derive a framework for incorporating DFIG-based wind power plants into load flow analysis of distribution systems. Several operational limits, including stator and rotor currents, were considered when determining the DFIG's active and reactive power (PQ) limits. Consequently, it is essential to calculate the rotor current for any operating speed using an appropriate equivalent circuit. The forward–reverse sweep method was used to determine the load flow solution. A non-iterative method for calculating steady-state operating points of DFIG-based wind energy systems is employed in [25]. This calculation is a crucial component of the stability analysis. Since it is assumed that the DFIG operates at a particular power factor, the bus to which it is connected must be treated as a PQ bus. Both sub-synchronous and super-synchronous modes of operation are analysed using distinct equivalent circuits. In [26], a direct or non-iterative method for calculating the steady-state operating points of a DFIG is proposed. This direct initialization method is applied to both sub-synchronous and super-synchronous modes using distinct models. This method has the benefit of preventing non-convergence issues and decreasing the calculation time for DFIG internal variables.

The study presented in [27] examines a hybrid renewable energy system that incorporates a DFIG in conjunction with a direct current (DC) motor. Two distinct equivalent circuits are employed to represent the DFIG, each corresponding to a specific operating speed. Initial values of a DFIM are computed using two distinct equivalent circuits dependent on the rotor speed in [28]. These values are utilized for the machine's dynamic simulation. To demonstrate the efficacy of the proposed equivalent circuits, time-domain simulations and eigenvalue analysis are presented. In accordance with the assertion put forth by [21, 22] that the equivalent circuit changes considerably depending on the operating speed, a new unbalanced steady-state model for DFIG operating at various speeds is presented in [29].

1.3. Necessity of the Research Based on Challenges of the Literature

The proposed circuit in [21, 22] for super-synchronous speeds differs from the well-established DFIM circuit derived in any course of electric machinery analysis for wound rotor induction machines [30, 31] and the well-established context on DFIM modelling and control [3]. The additional modelling complication introduced by using two different circuit models based on the operating slip is the second reason why using two different circuit models based on the operating slip is questionable, since an equivalent circuit may not apply for some values of slip. Moreover, the authors in [21, 22] have yet to present corrective measures to be taken when dealing with the dynamic *dq* model of the machine; in fact, their study is confined to steady-state phasor analysis of the machine.

1.4. Novelty and Main Contributions of the Paper

In this paper, it is demonstrated that while it is necessary to modify some relationships when the machine operates at super-synchronous speeds, it is neither necessary nor recommended that the well-established model be modified based on the operating speed: the same stator-referred equivalent circuit as for sub-synchronous speed can be used. The phasor diagram is then constructed based on the equivalent circuit, with negative slip taken into account. For the actual voltages and currents of the rotor side, it suffices to consider that when there is a negative slip, resulting in a negative rotor angular frequency ($s<0 \Rightarrow \omega_r<0$), the direction of rotation of rotor phasors is reversed relative to the direction of rotation of stator phasors (taking the normal direction to be counter-clockwise, the direction of rotation of rotor phasors for super-synchronous speeds will be clockwise). Therefore, only rotor reactive power expressions based on steady-state and dynamic equations should consider the rotor slip sign.

The primary contributions of the paper can be enumerated as follows:

- Providing a comprehensive understanding of the negative sequence phenomenon in the super-synchronous mode of operation.
- Proposal of a novel approach to address the change in phase sequence of rotor variables at super-synchronous speeds, which has implications for a number of established relationships.

➢ Criticism of changing the DFIM equivalent circuit based on rotor speed conditions (as done in [21, 22]). Alternatively, a unified modelling framework that can accommodate all operating speeds is proposed.

➢ Modifying some steady-state and dynamic relations to take super-synchronous speed into account, while resorting to the widely accepted equivalent circuit.

1.5. Organization and Structure of the Paper

This paper is organized as follows. In Section 2, a super-synchronous operation is investigated for the very special case of pure capacitive load at rotor terminals to shed some light on the problem. The general load case is then investigated in Section 3, which gives an insight into rotor reactive power expression based on the operational speed. Afterwards, in Section 4, phasor diagrams for the four-quadrant operation of a DFIM with unity stator power factor operation are illustrated and justified. Rotor reactive power under dynamic conditions is examined in Section 5. Section 6 contains simulation results and discussions, followed by conclusions.

2. Voltage-Current Relation for a Rotor Terminated With a Capacitive Load

To better illustrate the concept, consider a pure capacitive load connected to the rotor terminals of a DFIM rotating at super-synchronous speed as a particular case. In the given loading conditions, the relationship between the actual rotor phase voltage and current can be expressed by the following equation:

$$\bar{V}_r = \frac{-j}{C\omega_r}\bar{I}_r \tag{1}$$

where ω_r represents the electrical angular frequency of rotor variables. The over-barred variables ($\bar{V}_r$ and $\bar{I}_r$) denote phasors. Considering the negative sign of ω_r due to negative slip, the phasor diagram can be drawn, as shown in Fig. 1. The speed of rotation of the phasors corresponds to the rotor frequency. At first glance, it might look like the rotor voltage phasor leads the rotor current phasor in the figure. This cannot be correct because the load is pure capacitive. However, taking the actual direction of rotation of phasors, as expected for a capacitive load, the rotor current phasor is still leading the rotor voltage phasor, both rotating clockwise. The situation is best depicted in Fig. 2.

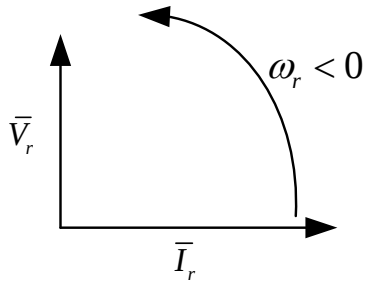

Fig. 1: Pure capacitive load phasor diagram for super-synchronous speed.

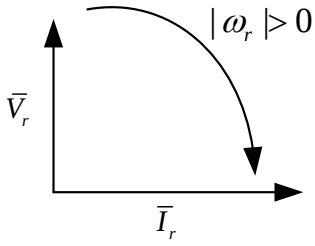

Fig. 2: Phasor diagram taking the actual direction of the phasors rotation.

The time variations of the voltage and current of rotor phase-a are expressed for better clarification. Assuming that the phase-a voltage at the rotor terminals is:

$$v_r(t) = V_{mr}\cos(\omega_r t) = V_{mr}\cos(s\,\omega_s t) \tag{2}$$

Rotor phase-a current is determined to be:

$$i_r(t) = C\frac{dv_r(t)}{dt} = cs\omega_s V_{mr}\cos(s\omega_s t + \frac{\pi}{2}) \tag{3}$$

where ω_s represents the electrical angular frequency of the stator. As the slip has been taken negative, the rotor voltage and current are expressed in an alternative way, resulting in the introduction of a positive frequency and the conversion of the negative multiplier of the cosine term in the rotor ($cs\omega_s < 0$) to a positive value:

$$v_r(t) = V_{mr}\cos(|\,s\,|\,\omega_s t), i_r(t) = c\,|\,s\,|\,\omega_s V_{mr}\cos(|\,s\,|\,\omega_s t + \frac{\pi}{2}) \tag{4}$$

This verifies the fact that the rotor current leads the rotor voltage.

It is now instructive to refer the rotor circuit to the stator (through frequency and turns-ratio transformations). The result is:

$$\frac{\bar{V}_r'}{s} = -\frac{j}{C's^2\omega_s}\bar{I}_r' \tag{5}$$

The above relation guarantees that the current of a pure capacitive load leads its voltage in the stator-referred equivalent circuit for both sub-synchronous and super-synchronous rotor speeds. A similar reasoning can be used to demonstrate that a pure inductive load connected to the rotor terminals will always have a current lagging its voltage, which is also supported in [32]. In fact, a capacitive (inductive) impedance is invariably capacitive (inductive), regardless of the operating speed. Instead of considering the rotor frequency to be negative when dealing with negative slips, it is preferable to consider the phase sequence to be reversed. The interested reader is referred to [33] for a more comprehensive examination of the negative frequency concept.

It is worth mentioning that the reactive power magnitude is increased on the stator side in comparison to the reactive power on the rotor side. This amplification of reactive power can be attributed to the division of frequency by slip when transforming from the rotor to the stator side.

In the rotor circuit, the reactive power produced by the capacitive load is:

$$Q_r = 3|\bar{V}_r||\bar{I}_r| \quad (6)$$

The stator-referred load also produces reactive power, and its value is determined by:

$$Q'_r = 3\left|\frac{\bar{V}'_r}{s}\right||\bar{I}'_r| = 3\frac{|\bar{V}'_r||\bar{I}'_r|}{|s|} = 3\frac{|\bar{V}_r||\bar{I}_r|}{|s|} = \frac{Q_r}{|s|} \quad (7)$$

The last expression shows that the reactive power produced by the capacitive reactance is amplified when the reactance is referred from its actual position (i.e., the rotor) to the stator side. This is supported by the expression of capacitive reactive power:

$$\begin{cases} Q_r = \dfrac{I_r^2}{C_r|\omega_r|} \\ Q'_r = \dfrac{I'^2_r}{C'_r\omega_s} = \dfrac{I_r^2}{C_r|s||\omega_r|} \end{cases} \Rightarrow Q'_r = \frac{Q_r}{|s|} \quad (8)$$

3. Voltage-Current Relation for the General Load Case

In the previous derivation, it was assumed that a pure capacitive load was connected to the rotor terminals of a DFIM operating at super-synchronous speed. Now, a general case will be examined. The relationship between rotor voltage and rotor current can be visualized more clearly with the aid of phasor diagrams, which depict the phasors of rotor voltage and current when they are on the rotor side and when they are referred to the stator side. Take the slip to be negative and assume that the rotor voltage and current phasors have a phase relationship when expressed in the actual rotor side, as shown in Fig. 3. As the slip is negative, the phasors rotate in a clockwise direction. Fig. 4 depicts the relative position of the stator-referred phasors appearing in the equivalent circuit. The direction of rotation of the phasors has now been reversed, and it is in the normal counter-clockwise direction. The referred rotor voltage phasor ($\bar{V}'_r/s$) is in the opposite

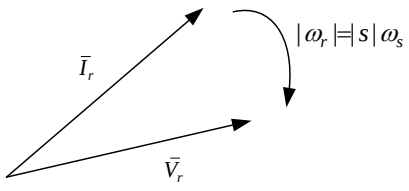

Fig. 3: Rotor phasors at super-synchronous speed.

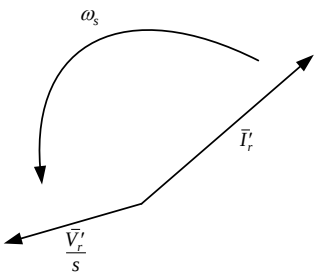

Fig. 4: Stator-referred rotor phasors.

direction with respect to the rotor voltage phasor ( ) as a result of a negative slip.

It is evident that in case the rotor voltage phasor leads the rotor current phasor on the rotor side, the referred rotor voltage phasor in the equivalent circuit (denoted as: $\bar{V}'_r/s$) also leads the referred rotor current phasor ($\bar{I}'_r$), regardless of whether the operation is in sub-synchronous or super-synchronous mode. It is observed that the relative position of the two phasors does not change if the rotational direction of the respective phasors is considered. This explanation confirms the intuitive expectation that the sign of reactive power from the rotor-side converter (RSC) to the rotor is identical to the sign of reactive power from the stator-referred rotor voltage source ($\bar{V}'_r/s$) to the stator-referred equivalent circuit, regardless of the operating mode, motoring or generating, sub-synchronous or super-synchronous speeds. This is shown schematically in Figs. 5a and 5b, in which the two reactive powers always have the same sign and differ only in magnitude ($Q'_r = Q_r/|s|$). The aforementioned expectation is consistent with [32], but the reactive power flow diagram in [34] ignores this fact, resulting in incompatible outcomes for super-synchronous speeds.

4. Phasor Diagrams for the Four-Quadrant Operation of DFIM

In this section, phasor diagrams are drawn for a DFIM operating at unity stator power factor (zero stator reactive power). The diagrams are drawn for all four quadrants pertaining to the direction of stator active power and the slip sign. Therefore, the machine can operate in motoring/generating mode with sub/super-synchronous rotor speeds.

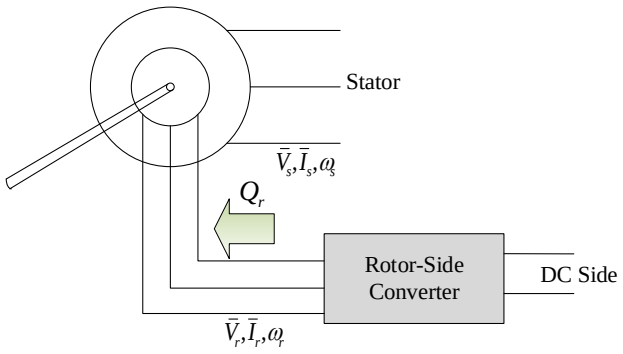

(a)

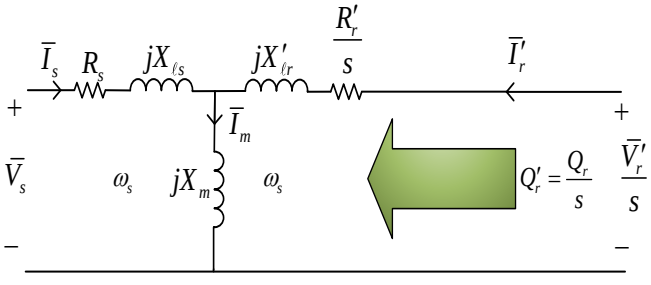

(b)

Fig. 5: (a) actual reactive power supplied into the rotor windings from the RSC, (b) reactive power supplied into the stator-referred equivalent circuit.

It is noteworthy in Fig. 6 that for sub-synchronous modes ((a) and (c)), the rotor angular frequency takes a positive value ($\omega_r > 0$), indicating that the phasors of actual (not stator-referred) rotor variables ($\bar{V}_r, \bar{I}_r, \bar{\psi}_r$) rotate in the same direction as the stator variables. In contrast, for super-synchronous modes ((b) and (d)), the slip and the rotor angular frequency become negative ($\omega_r < 0$); consequently, the direction of rotation of rotor phasors is reversed. All phasors associated with stator variables and rotor variables referred to the stator rotate at an angular frequency of ω_s.

The governing phasor equations in Fig. 5b are as follows:

$$\bar{V}_s = R_s \bar{I}_s + j\omega_s \bar{\psi}_s \tag{9}$$

$$\bar{\psi}_s = L_s \bar{I}_s + L_m \bar{I}'_r \tag{10}$$

$$\bar{V}'_r = R_r \bar{I}'_r + j\omega_r \bar{\psi}'_r \tag{11}$$

$$\bar{\psi}'_r = L_r \bar{I}'_r + L_m \bar{I}_s \tag{12}$$

In the following, a number of noteworthy findings in relation to the four quadrants illustrated in Fig. 6 are presented.

- Parts (a) and (b) represent motoring mode with a unity power factor; consequently, motoring convention dictates that the stator current phasor and stator voltage phasor are in phase. In contrast, the stator current phasor is 180 degrees out of phase with the stator voltage phasor in parts (c) and (d) corresponding to the generating mode.
- In motoring mode, the stator flux linkage phasor leads the rotor flux linkage phasor (referred to the stator). The opposite is true for generating mode.
- The angle between stator-referred rotor voltage and current phasors in parts (b) and (c), i.e., super-synchronous motoring and sub-synchronous generating modes, is less than 90 degrees. These two modes of operation are actually incompatible with a conventional induction machine with a shorted rotor winding. Consequently, these two new modes of DFIM operation require injection of active power into the rotor windings through an external circuit (the RSC).
- Assuming the stator's reactive power is zero and considering the reactive power requirement for core magnetization, one would expect that reactive power should be supplied to the rotor winding by the RSC in all four quadrants. From the viewpoint of the phasor diagram, the rotor current phasor should lag the rotor voltage phasor. Taking into account the positive direction of rotor phasors rotation in parts (a) and (c), it is evident that the rotor current phasor lags the rotor voltage phasor. Also, in parts (b) and (d), when the reverse rotational direction of the rotor phasors is considered (due to negative ω_r), it is again interestingly observed that the rotor current phasor lags the rotor voltage phasor. This signifies the injection of reactive power into the rotor.

The validity of the phasor diagram results is supported by the consistency with physical considerations. It is worth noting that the phasor diagrams for all four quadrants in this study have been drawn using the same equivalent circuit, as shown in Fig. 5b. On the contrary, an alternative equivalent circuit has been utilised in [21, 22] to represent super-synchronous operating modes. This in turn increases the complexity of the problem and, if care is not taken in selecting the correct equivalent circuit, could lead to incorrect results.

5. Expression of Reactive Power Based on the Dynamic Model

Up to now, the focus has been on the steady-state expression of the reactive power, employing phasor equations and the steady-state equivalent circuit. Expression of the equations in the synchronous *dq* reference frame is useful for gaining insight into the conditions that prevail under transient conditions. The *dq* transformation is implemented to investigate the relationship between the actual rotor side and stator-referred reactive powers. The particular steady-state case is taken into account as the primary objective is to determine the relative signs of reactive powers. Here, the same power-invariant *abc* to *dq* transformation is used as in [21, 22] in order to facilitate a comparison between the method presented in this paper and what has been presented in [21, 22].

Assuming that the rotor voltages are a balanced positive sequence set, they are referred to the synchronous reference frame (see (13)) where θ_s is the angle of the synchronous frame, θ_m is the rotor angle with respect to the stationary phase-a axis, and θ_0 is an initial phase angle, all expressed in electrical radians.

The slip angle can now be expressed as given by (14), where ω_r is the slip speed (which is also the angular frequency of the rotor voltages) in electrical radians/s.

$$\theta_r = \theta_s - \theta_m = \omega_r t \tag{14}$$

Recall that the rotor angular frequency was assumed to be positive ($\omega_r > 0$) in order to have positive sequence rotor voltages.

$$\begin{bmatrix} v_{dr} \\ v_{qr} \\ v_{0r} \end{bmatrix} = \sqrt{\frac{2}{3}} \begin{bmatrix} \cos(\theta_s - \theta_m) & \cos(\theta_s - \theta_m - \frac{2\pi}{3}) & \cos(\theta_s - \theta_m - \frac{4\pi}{3}) \\ -\sin(\theta_s - \theta_m) & -\sin(\theta_s - \theta_m - \frac{2\pi}{3}) & -\sin(\theta_s - \theta_m - \frac{4\pi}{3}) \\ \frac{1}{\sqrt{2}} & \frac{1}{\sqrt{2}} & \frac{1}{\sqrt{2}} \end{bmatrix} \begin{bmatrix} V_{rm}\cos(\omega_r t + \theta_0) \\ V_{rm}\cos(\omega_r t + \theta_0 - \frac{2\pi}{3}) \\ V_{rm}\cos(\omega_r t + \theta_0 - \frac{4\pi}{3}) \end{bmatrix} \tag{13}$$

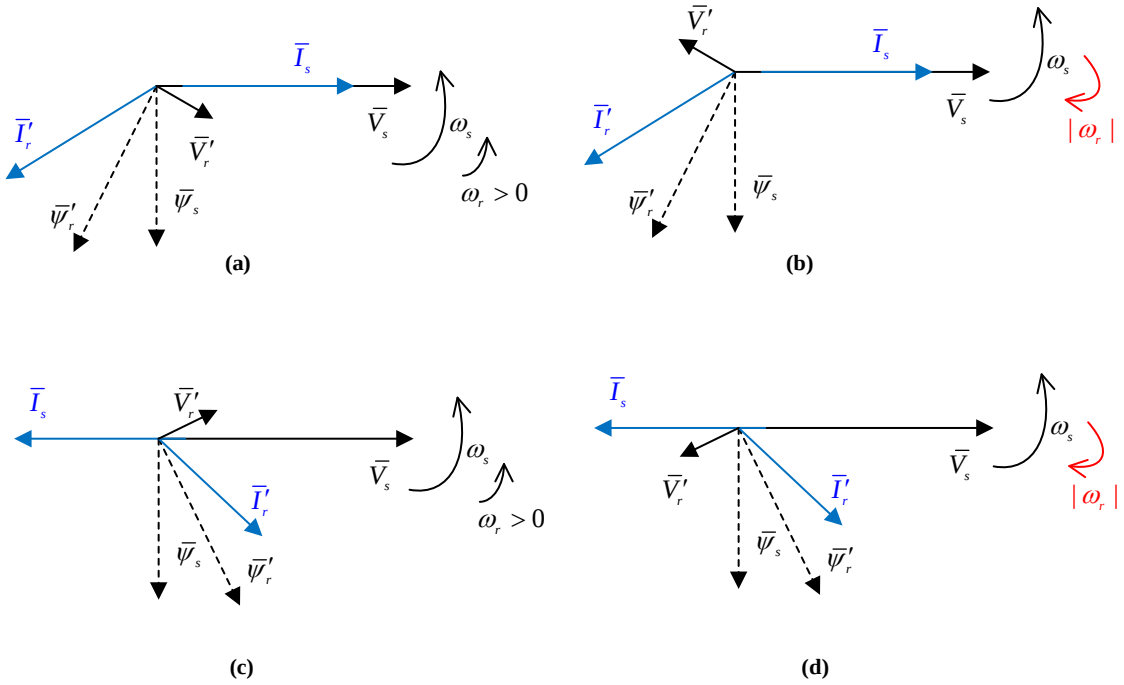

Fig. 6: Phasor diagram of DFIM for four quadrants (with unity stator power factor). (a) sub-synchronous motoring, (b) super-synchronous motoring, (c) sub-synchronous generating, (d) super-synchronous generating.

Using (13), the *dq* components of the rotor voltage can be easily determined. The result is:

$$v_{dr} = \sqrt{\frac{3}{2}} V_{rm} \cos(\theta_0), v_{qr} = \sqrt{\frac{3}{2}} V_{rm} \sin(\theta_0) \tag{15}$$

Because the voltages are assumed to be balanced, there will be no zero-sequence component ($v_{0r} = 0$).

The rotor voltage phasor can now be expressed using the d-axis and q-axis components in the synchronous reference frame, resulting in:

$$\bar{V}_r = v_{dr} + j v_{qr} = \sqrt{\frac{3}{2}} V_{rm} e^{j\theta_0} \tag{16}$$

It is observed that for ($\omega_r > 0$), a three-phase positive sequence rotor voltage set is converted to DC values in the synchronous reference frame.

Assuming that each rotor phase current lags its corresponding phase voltage by an angle of (φ), the three-phase rotor currents are represented as follows:

$$\begin{cases} i_{ar} = I_{rm} \cos(\omega_r t + \theta_0 - \varphi) = I_{rm} \cos(\omega_r t + \gamma) \\ i_{br} = I_{rm} \cos(\omega_r t + \gamma - \frac{2\pi}{3}) \\ i_{cr} = I_{rm} \cos(\omega_r t + \gamma - \frac{4\pi}{3}) \end{cases} \tag{17}$$

where γ has been defined to be: $\gamma = \theta_0 - \varphi$.

The *dq* components of the rotor current are derived as follows:

$$i_{dr} = \sqrt{\frac{3}{2}} I_{rm} \cos(\gamma),\ i_{qr} = \sqrt{\frac{3}{2}} V_{rm} \sin(\gamma) \tag{18}$$

Using (18), the following expression represents the rotor current phasor:

$$\bar{I}_r = i_{dr} + j i_{qr} = \sqrt{\frac{3}{2}} I_{rm} e^{j(\theta_0 - \varphi)} \tag{19}$$

Since the transformation is power-invariant, the active and reactive powers supplied into the rotor are expressed as follows:

$$\begin{aligned} P_r &= real(\bar{V}_r \bar{I}_r^*) = (\frac{3}{2}) V_{rm} I_{rm} \cos(\varphi) = v_{dr} i_{dr} + v_{qr} i_{qr} \\ Q_r &= imag(\bar{V}_r \bar{I}_r^*) = (\frac{3}{2}) V_{rm} I_{rm} \sin(\varphi) = v_{qr} i_{dr} - v_{dr} i_{qr} \end{aligned} \tag{20}$$

In the preceding derivations ((13)-(20)), a sub-synchronous mode of operation corresponding to ($\omega_r > 0$) was assumed. As a next step, the super-synchronous mode of operation is studied. In this mode corresponding to ($\omega_r < 0$), the rotor voltages with the same expression will appear as a negative sequence set:

$$\begin{cases} v_{ar} = V_{rm} \cos(\omega_r t + \theta_0) = V_{rm} \cos(|\omega_r| t - \theta_0) \\ v_{br} = V_{rm} \cos(\omega_r t + \theta_0 - \frac{2\pi}{3}) = V_{rm} \cos(|\omega_r| t - \theta_0 + \frac{2\pi}{3}) \\ v_{cr} = V_{rm} \cos(\omega_r t + \theta_0 - \frac{4\pi}{3}) = V_{rm} \cos(|\omega_r| t - \theta_0 + \frac{4\pi}{3}) \end{cases} \tag{21}$$

The exact same d-axis and q-axis voltage components and rotor voltage phasor are obtained for negative sequence

voltages when they are transformed to the synchronous reference frame ((15) and (16)).

Now, the rotor currents at super-synchronous speed are expressed in their *abc* reference frame and then transformed to the synchronous reference frame. Again, it is supposed that the rotor phase current lags the phase voltage by an angle of (φ).

$$\begin{aligned} &v_{ar} = V_{rm}\cos(\omega_r t+\theta_0) = V_{rm}\cos(|\omega_r|t-\theta_0) \Rightarrow \\ &i_{ar} = I_{rm}\cos(|\omega_r|t-\theta_0-\varphi) = I_{rm}\cos(\omega_r t+\theta_0+\varphi) \end{aligned} \quad (22)$$

Similarly:

$$\begin{aligned} &v_{br} = V_{rm}\cos(\omega_r t+\theta_0-\frac{2\pi}{3}) = V_{rm}\cos(|\omega_r|t-\theta_0+\frac{2\pi}{3}) \\ &\Rightarrow i_{br} = I_{rm}\cos(|\omega_r|t-\theta_0+\frac{2\pi}{3}-\varphi) = \ldots \\ &\quad I_{rm}\cos(\omega_r t+\theta_0+\varphi-\frac{2\pi}{3}) \end{aligned} \quad (23)$$

and:

$$i_{cr} = I_{rm}\cos(\omega_r t+\theta_0+\varphi-\frac{4\pi}{3}) \quad (24)$$

Defining ($\gamma = \theta_0+\varphi$), the rotor currents are transformed to the synchronous reference frame, resulting in:

$$i_{dr} = \sqrt{\frac{3}{2}}I_{rm}\cos(\gamma),\ i_{qr} = \sqrt{\frac{3}{2}}V_{rm}\sin(\gamma) \quad (25)$$

Finally, the rotor current phasor is derived as follows:

$$\bar{I}_r = i_{dr} + j i_{qr} = \sqrt{\frac{3}{2}}I_{rm}e^{j(\theta_0+\varphi)} \quad (26)$$

Considering (16) and (26), it can be seen that, for super-synchronous operation, if the rotor phase currents lag (lead) their respective phase voltages by an angle of φ, the *dq* rotor currents will lead (lag) their respective *dq* rotor voltages by the same angle.

Since the relative angle between the rotor phase voltage and current has not changed (it can be assumed that a load is connected to the rotor terminals to fix the relative angles), it is expected that the rotor active and reactive powers remain the same as they were when the rotor was rotating at sub-synchronous speed. Manipulation of the *dq* voltage and current expressions ((15), (16), (25), and (26)) yields:

$$\begin{aligned} &P_r = (\frac{3}{2})V_{rm}I_{rm}\cos(\varphi) = real(\bar{V}_r\bar{I}_r^*) = v_{dr}i_{dr}+v_{qr}i_{qr} \\ &Q_r = (\frac{3}{2})V_{rm}I_{rm}\sin(\varphi) = -imag(\bar{V}_r\bar{I}_r^*) = -(v_{qr}i_{dr}-v_{dr}i_{qr}) \end{aligned} \quad (27)$$

Equation (27) demonstrates that while the expression for rotor active power is independent of whether the rotor is operating in sub-synchronous or super-synchronous mode, for the reactive power supplied to the rotor, it is important to consider whether the speed is sub-synchronous (where (20) is valid) or super-synchronous (where (27) is valid).

It is advisable not to modify the equivalent circuit referred to the stator and the phasor diagram based on this circuit in accordance with the operating speed of the machine. Rather, while other relationships remain unchanged for super-synchronous speed, the expression for reactive power supplied into the rotor of the DFIM from the RSC should be modified. The following general expression for rotor reactive power is proposed for use at all operating speeds:

$$Q_r = sign(s)*imag(\bar{V}_r\bar{I}_r^*) = sign(s)*(v_{qr}i_{dr}-v_{dr}i_{qr}) \quad (28)$$

The coefficient ($sign(s)$) in (28) accounts for sub-synchronous (positive slip, therefore $sign(s)=1$) and super-synchronous (negative slip, therefore $sign(s)=-1$) speeds.

6. Results and Discussion

To demonstrate the effectiveness of the proposed rotor reactive power relation given by (28), a DFIM with the specifications listed in Table 1 is simulated in Matlab® Simulink under vector control using reference values of rotor speed and stator reactive power. The mechanical torque is taken as the input to the system. This could be load torque in the case of a motor or turbine torque in the case of a generator. As per the adopted motoring convention, positive values of mechanical torque and stator active power indicate motoring operation, whereas negative values of these variables indicate generation. In accordance with [21], the reference stator reactive power is kept at zero in order for the machine to be magnetized through the rotor; in other words, under this control scenario, positive reactive power must be supplied to the rotor in various operating modes. For the first 15 seconds, the reference speed is maintained at 0.7 pu (i.e., sub-synchronous speed), and then it changes to 1.3 pu (i.e., super-synchronous speed). Fig. 7 shows the active and reactive powers supplied into the stator winding for motoring operation. To simulate this mode of operation, a positive value of input torque (load torque) was used. Given the objective of this paper, which is not centered around control of the system's performance, transients occurring in the waveforms are not deemed important and emphasis is made on their steady-state values. Fig. 8 depicts the variation of rotor *abc* currents when in motoring mode at two distinct operating speeds. On the left side of the figure, corresponding to the sub-synchronous speed, the currents indicate a positive sequence. Conversely, on the right side of the figure, corresponding to the super-synchronous speed, the currents indicate a negative sequence. The same phase reversal phenomenon is observed for rotor voltages as well (Fig. 9). Fig. 10 illustrates the relative time displacement of the rotor phase-a voltage and current waveforms for motoring operation at sub-synchronous (left) and super-synchronous (right) speeds. It is interesting to note that the rotor current always lags the rotor voltage, regardless of the operating speed. This was expected because, with the stator's reactive power maintained at zero, the DFIM should be magnetized

Table 1: Specifications of the simulated DFIM.

Parameter	Unit	Value
Stator resistance	pu	0.05
Rotor resistance	pu	0.02
Stator leakage inductance	pu	0.1
Rotor leakage inductance	pu	0.1
Magnetizing inductance	pu	5
Base frequency	Hz	60

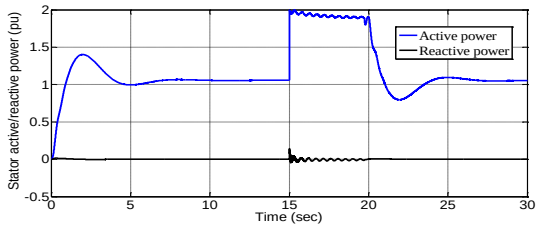

Fig. 7: Stator active and reactive powers for positive input torque (motoring operation).

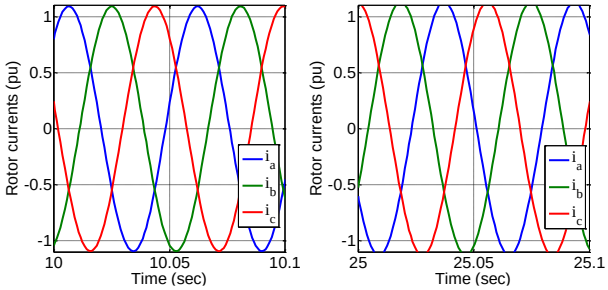

Fig. 8: Rotor phase currents for motoring mode (left: sub-synchronous, right: super-synchronous).

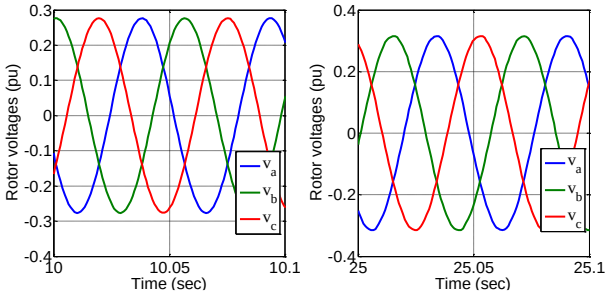

Fig. 9: Rotor phase voltages for motoring mode (left: sub-synchronous, right: super-synchronous).

through the rotor; therefore, from the standpoint of the RSC, the rotor is inductive. For sub-synchronous speed (left), the rotor current lags the rotor voltage by more than 90 degrees, indicating that the rotor active power is negative (power supplied from the rotor to the RSC). In contrast, for super-synchronous speed (right), the rotor current lags the rotor voltage by an angle less than 90 degrees, indicating that the rotor active power is positive (power supplied into the rotor from the RSC). This is consistent with what has been reported in the literature [3]. Fig. 11 shows a comparison between the reactive power of the rotor calculated with the traditional equation (20) and the modified equation (28). Clearly, the rotor's steady-state reactive power must be positive for the machine to be magnetized. While both expressions produce similar results for sub-synchronous speeds, only the modified relation derived in this paper yields the correct rotor reactive power for super-synchronous speeds.

Fig. 12 shows the variation of stator active and reactive powers during generating operation. This mode of operation is achieved by keeping the input torque (turbine torque) negative. Fig. 13 depicts the variation of rotor *abc* currents in generating mode, where the phase sequence of rotor currents changes as the speed changes from sub-synchronous (left) to super-synchronous (right). This behavior was also observed for motoring operation (Fig. 8). As seen in Fig. 14, when the

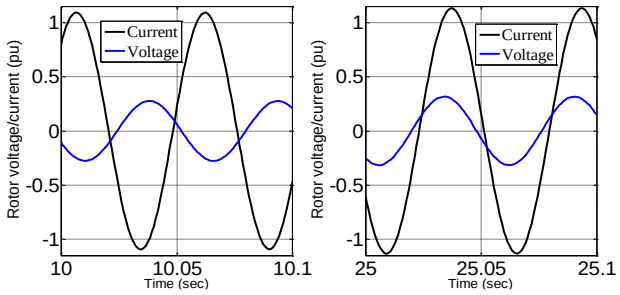

Fig. 10: Relative time displacement of rotor voltage and current for motoring mode (left: sub-synchronous, right: super-synchronous).

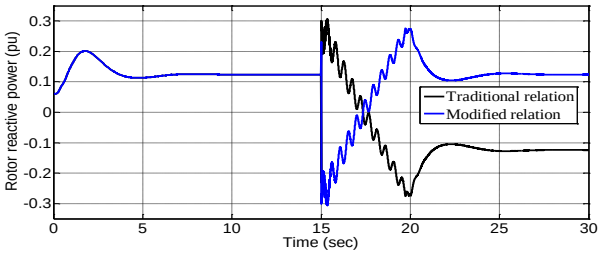

Fig. 11: Rotor reactive power using traditional and modified relations (motoring operation).

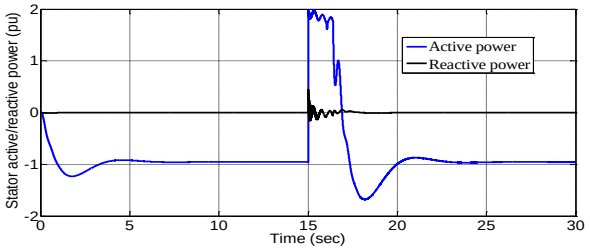

Fig. 12: Stator active and reactive powers for negative input torque (generating operation).

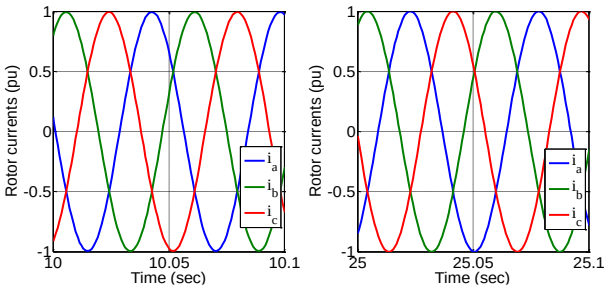

Fig. 13: Rotor phase currents for generating mode (left: sub-synchronous, right: super-synchronous).

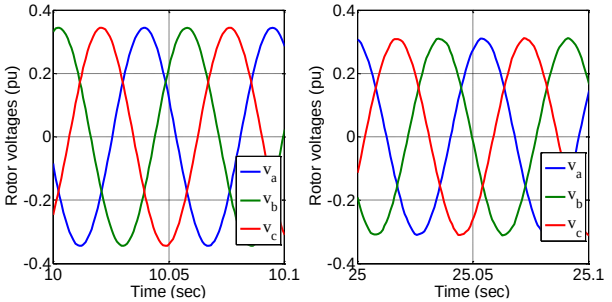

Fig. 14: Rotor phase voltages for generating mode (left: sub-synchronous, right: super-synchronous).

rotor speed goes from sub-synchronous to super-synchronous, the sequence of rotor voltages also changes. Variation of rotor phase-a voltage and current for generating operation is illustrated in Fig. 15 for both sub-synchronous (left) and super-synchronous (right) speeds. Similar to Fig. 10, rotor current lags rotor voltage under both conditions for the same reason.

For sub-synchronous generating operation, active power must be supplied to the rotor windings, necessitating a phase angle difference of less than 90 degrees between rotor voltage and current (left); for super-synchronous generating operation, active power must be drawn from the rotor to the RSC, necessitating a phase angle difference of greater than 90 degrees (right). This is again consistent with [3]. As was done for the motoring mode, the traditional and modified rotor reactive power expressions are compared for the generating mode in Fig. 16. Again, it is evident that both relations produce identical results for sub-synchronous speeds. Nonetheless, only the modified relation provides the correct sign of reactive power for super-synchronous speeds. To validate the proposed modified rotor reactive power relation (28) further, the reactive power requirement of the rotor for various stator reactive powers is obtained under super-synchronous rotor speeds for both motoring and generating modes, and indicated in Fig. 17. The predictions from the proposed method and the existing reactive power relation are both drawn for the sake of comparison. The flowchart of computations using the proposed method is depicted in Fig. 18. For a DFIM with parameters given in Table 1, super-synchronous operating mode with ($s = -0.25$) is investigated using the proposed modified relation and the traditional relation. The stator voltage is assumed to be $1\angle 0^\circ\ pu$. For this scenario, the stator side active power is taken to be $\pm 0.9\ p.u.$ (positive for motoring and negative for generating operation). Stator reactive power is allowed to vary in the range $Q_{\min} \le Q_s \le Q_{\max}$ and the variation of rotor reactive power is investigated. Taking the equivalent circuit of DFIM into account, as the inductive elements in the circuit absorb reactive power, there is need of reactive power from the rotor side ($Q_r > 0$) to magnetize the machine when the stator feeds reactive power to the grid ($Q_s < 0$). This is in accordance with the predictions from the proposed formulation, but in contrast to the predictions of the traditional formulation, confirming the validity of the proposed method.

6.1. Sensitivity Analysis

For further analysis, the sensitivity of rotor reactive power direction to parameter changes (which can occur due to temperature rise or saturation effects) is investigated by varying the magnetizing inductance (L_m) and computing Q_r with respect to Q_s for motoring and generating modes, as illustrated in Fig. 19 and Fig. 20, respectively. The DFIM is again assumed to be at super-synchronous mode of operation ($s = -0.25$) with a stator voltage of $1\angle 0^\circ\ pu$. It is clear that the impact of machine parameter changes on rotor reactive power direction is minimal.

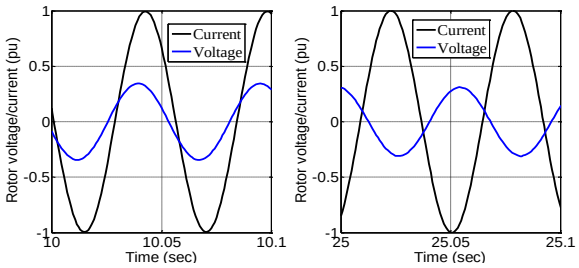

Fig. 15: Relative time displacement of rotor voltage and current for generating mode (left: sub-synchronous, right: super-synchronous).

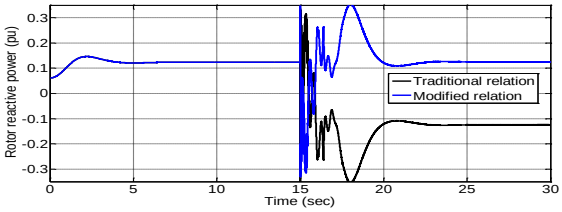

Fig. 16: Rotor reactive power using traditional and modified relations (generating operation).

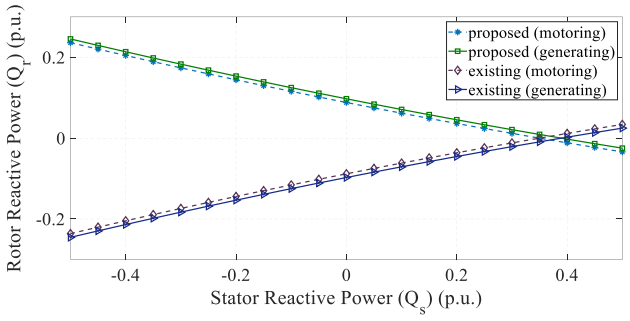

Fig. 17: Rotor reactive power versus stator reactive power for super-synchronous operation ($P_s = 0.9\ pu$ for motoring mode and $P_s = -0.9\ pu$ for generating mode).

7. Conclusion

A comprehensive investigation into the impact of super-synchronous operation of DFIMs on rotor reactive power was provided in this paper. Under such operating conditions, the slip is negative, causing the rotor frequency to be negative. Clearly, a negative rotor frequency has no physical significance, but it does indicate a change of the phase sequence of rotor voltages and currents. It has been demonstrated that the well-established stator-referred equivalent circuit of DFIM is valid for both sub-synchronous and super-synchronous speeds; yet, care must be taken when dealing with phasor diagrams drawn for super-synchronous speeds, where the actual rotor variables rotate in the opposite direction to the stator-referred variables. Also, when calculating rotor reactive power using *dq* rotor variables, the traditional relation must be modified to account for the sign of slip. While the focus of this article was on conventional (brushed) doubly fed induction machines, the scope of the study can be extended to include other types of doubly fed machines, such as brushless doubly fed machines with

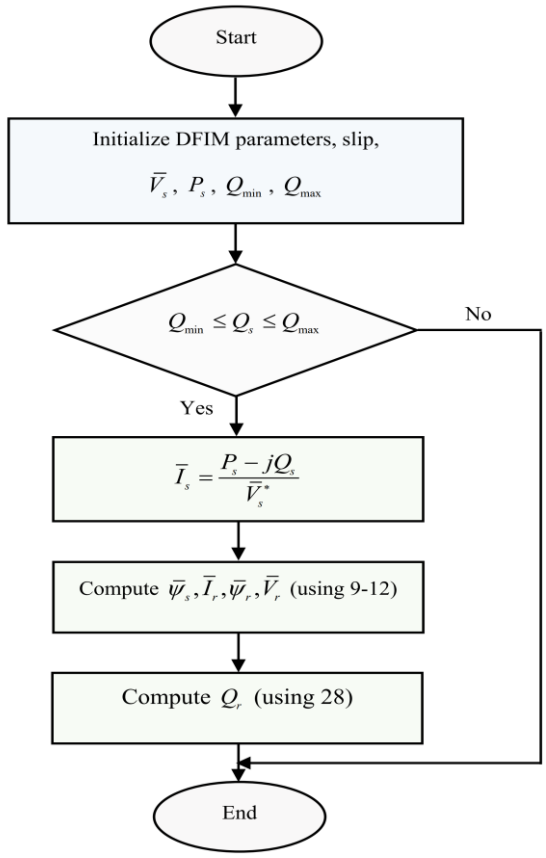

Fig. 18: Flowchart of Q_r versus Q_s calculation for $Q_{min} \le Q_s \le Q_{max}$ at a predefined slip and fixed P_s and $\bar{V}_s$.

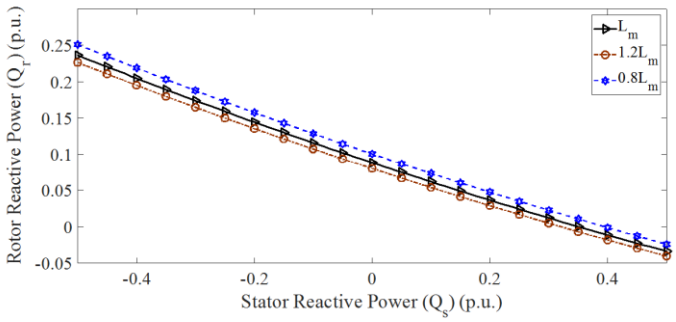

Fig. 19: Impact of variation of magnetizing inductance on rotor reactive power for motoring mode ($P_s = 0.9\ pu$).

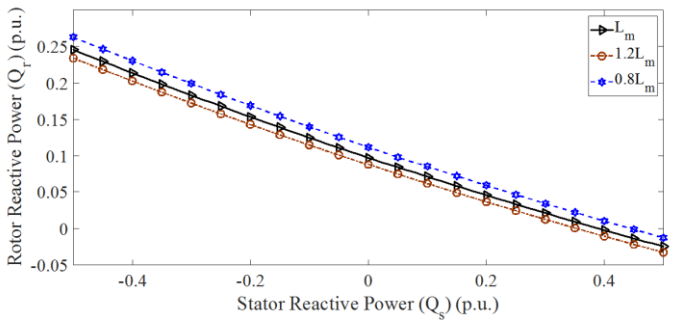

Fig. 20: Impact of variation of magnetizing inductance on rotor reactive power for generating mode ($P_s = -0.9\ pu$).

induction or reluctance rotors. These electromechanical converters enjoy comparable advantages of a fractionally rated converter like the DFIM. Simultaneously, they eliminate the need for brushes and slip rings found in the DFIM, rendering them more maintenance-free. A comparable frequency conversion method is utilised for their modelling, where the parameters of the secondary stator winding are referred to the primary stator winding. Future research is going to focus on investigating the reactive power relation of the secondary winding, taking the potential reversal in phase sequence of its voltages and currents into account.

CRediT Authorship Contribution Statement

Mohammad Naser Hashemnia: Conceptualization, Data curation, Formal analysis, Funding acquisition, Investigation, Methodology, Project administration, Resources, Software, Supervision, Validation, Visualization, Roles/Writing - original draft, Writing - review & editing.

Declaration of Competing Interest

The authors declare that they have no known competing financial interests or personal relationships that could have appeared to influence the work reported in this paper. The ethical issues; including plagiarism, informed consent, misconduct, data fabrication and/or falsification, double publication and/or submission, redundancy has been completely observed by the authors.

References

[1] A. K. Abdulabbas, M. A. Alawan, and D. K. Shary, "Limits of reactive power compensation of a doubly fed induction generator based wind turbine system," *Bulletin of Electrical Engineering and Informatics*, vol. 12, no. 5, pp. 2521–2534, Oct. 2023.

[2] F. Z. Messaoud, T. Hamza, B. Ouamri, M. Abasi, and A. R. Zerek, "Decoupled SMC of DFIG Based Multi-Level Inverter," in *2021 IEEE 1st International Maghreb Meeting of the Conference on Sciences and Techniques of Automatic Control and Computer Engineering (MI-STA)*, May 2021.

[3] G. Abad, J. López, M. Rodríguez, L. Marroyo, and G. Iwanski, *Doubly fed induction machine: modeling and control for wind energy generation*. Oxford: Wiley-Blackwell, 2011.

[4] L. Fan, and Z. Miao, *Modeling and Analysis of Doubly Fed Induction Generator Wind Energy Systems*. Academic Press, 2015.

[5] E. N. Sanchez and Riemann Ruiz-Cruz, *Doubly Fed Induction Generators*. CRC Press, 2016.

[6] D. Xu, F. Blaabjerg, W. Chen, and N. Zhu, *Advanced control of doubly fed induction generator for wind power systems*. Hoboken, New Jersey John Wiley Et Sons, 2018.

[7] A. Abdelbaset, Y. S. Mohamed, A.-H. M. El-Sayed, A. E. Hussein, and A. Ahmed, *Wind Driven Doubly Fed Induction Generator*. Springer, 2017.

[8] A. Sguarezi, *Model Predictive Control for Doubly-Fed Induction Generators and Three-Phase Power Converters*. Elsevier, 2022.

[9] A. Dòria-Cerezo, M. A. Hossain, and M. Bodson, "Complex-Valued Sliding Mode Controllers for Doubly-Fed Induction Motors," *IEEE Transactions on Control Systems and Technology*, vol. 31, no. 3, pp. 1336–1344, May 2023.

[10] F. Pourmirzaei-Deylami, and A. Darabi, "Steady-state performance analysis for optimal operation determination of doubly fed induction motors," *The Journal of Engineering*, Dec. 2022.

[11] M. Zerzeri, A. Khedher, and F. Jallali, "Steady-state characteristics of DFIM : the potentialities of integration in electrical traction systems," *Research Square (Research Square)*, Feb. 2023.

[12] X. Roboam, "A review of powertrain electrification for greener aircraft," *Energies*, vol. 16, no. 19, p. 6831, Jan. 2023.

[13] S. Li, "Converters loading balance and stability verification for doubly-fed induction generator," *CSEE Journal of Power and Energy Systems*, 2022.

[14] R. Gianto, "Steady-state model of DFIG-based wind power plant for load flow analysis," *IET Renewable Power Generation*, Mar. 2021.

[15] R. Gianto, K. H. Khwee, H. Priyatman, and M. Rajagukguk, "Two-port network model of fixed-speed wind turbine generator for distribution system load flow analysis, " *Telecommunication Computing Electronics and Control (TELKOMNIKA)*, vol. 17, no. 3, p. 1569, Jun. 2019.

[16] R. Gianto, "Constant voltage model of DFIG-based variable speed wind turbine for load flow analysis," *Energies*, vol. 14, no. 24, p. 8549, Dec. 2021.

[17] R. Gianto, "Constant power factor model of DFIG-Based wind turbine for steady state load flow studies," *Energies*, vol. 15, no. 16, pp. 6077–6077, Aug. 2022.

[18] R. Gianto, "Integration of DFIG-Based variable speed wind turbine into load flow analysis," in *2021 International Seminar on Intelligent Technology and Its Applications (ISITIA)*, 2021, pp. 63-66.

[19] K. H. Shin, and T. A. Lipo, "A super-synchronous doubly fed induction generator option for wind turbine applications," in *2016 IEEE Energy Conversion Congress and Exposition (ECCE)*, 2016, pp. 1-7.

[20] T. H. Ortmeyer, "Negative frequency aspects of doubly fed machine analysis," *Proceedings of the IEEE*, vol. 71, no. 8, pp. 1017-1017, Aug. 1983.

[21] V. S. S. Kumar, and D. Thukaram, "Accurate steady-state representation of a doubly fed induction machine," *IEEE Transactions on Power Electronics*, vol. 30, no. 10, pp. 5370-5375, Oct. 2015.

[22] V. S. S. Kumar, and D. Thukaram, "Alternate proof for steady-state equivalent circuit of a doubly fed induction machine," *IEEE Transactions on Power Electronics*, vol. 31, no. 8, pp. 5378-5383, Aug. 2016.

[23] V. S. S. Kumar, and D. Thukaram, "Accurate modeling of doubly fed induction generator based wind farms in load flow analysis," *Electric Power Systems Research*, vol. 155, pp. 363–371, Feb. 2018.

[24] C.V.S. Anirudh, and V. S. S. Kumar, "Enhanced modelling of doubly fed induction generator in load flow analysis of distribution systems," *IET Renewable Power Generation*, vol. 15, no. 5, pp. 980–989, Jan. 2021.

[25] D. R. Karthik, and S. M. Kotian, "Initialization of doubly-fed induction generator wind turbines using noniterative method," in *2019 8th International Conference on Power Systems (ICPS)*, 2019, pp. 1-6.

[26] D. R. Karthik, S. M. Kotian, and N. S. Manjarekar, "A direct method for calculation of steady-state operating conditions of a doubly fed induction generator," in *2021 9th IEEE International Conference on Power Systems (ICPS)*, 2021, pp. 1-6.

[27] Y. V. Pavan Kumar, and R. Bhimasingu, "Performance analysis of static versus rotary DC/AC power converters for hybrid renewable energy based microgrid applications," in *2016 IEEE Region 10 Conference (TENCON)*, 2016, pp. 1456-1461.

[28] V. S. Sravan Kumar, "Computation of initial conditions for dynamic analysis of a doubly fed induction machine based on accurate equivalent circuit," in *2019 IEEE International Electric Machines & Drives Conference (IEMDC)*, 2019, pp. 307-313.

[29] Y. Ju, F. Ge, W. Wu, Y. Lin, and J. Wang, "Three-phase steady-state model of doubly fed induction generator considering various rotor speeds," *IEEE Access*, vol. 4, pp. 9479-9488, 2016.

[30] P. C. Krause, Oleg Wasynczuk, S. D. Sudhoff, S. Pekarek, and Institute Of Electrical And Electronics Engineers, *Analysis of electric machinery and drive systems*. Hoboken, New Jersey: Wiley, 2013.

[31] P. C. Krause and T. R. Krause, *Introduction to modern analysis of electric machines and drives*. John Wiley & Sons, 2022.

[32] T. J. E. Miller, "Theory of the doubly-fed induction machine in the steady state," in *XIX International Conference on Electrical Machines (ICEM 2010)*, 2010, pp. 1-6.

[33] G. T. Heydt, "The meaning, analysis, and consequences of negative frequency in electric power systems," in *2022 North American Power Symposium (NAPS)*, 2022, pp. 1-6.

[34] N. Bianchi, L. Alberti and S. Bolognani, "A design-oriented model of doubly-fed induction machine,"in *2011 IEEE International Electric Machines & Drives Conference (IEMDC)*, 2011, pp. 557-562.

BIOGRAPHY

Mohammad Naser Hashemnia was born in Mashhad, Iran, in 1983. He received the B.S. degree in electrical power engineering from Ferdowsi University, Mashhad, Iran, in 2006 and the M.S. degree in electrical power engineering from the University of Tehran, Tehran, Iran, in 2008. He got his Ph.D. degree in electrical power engineering from Sharif University of Technology, Tehran, Iran in 2013. Since 2015 he has been an assistant professor in Mashhad branch, Islamic Azad University, Mashhad, Iran. His main research interests include analysis, modelling and simulation of electric machines, advanced control methods for electrical drives and renewable energy systems.